A HYBRID MULTISCALE MODEL FOR CANCER INVASION OF THE EXTRACELLULAR MATRIX

NIKOLAOS SFAKIANAKIS*, ANOTIDA MADZVAMUSE†, AND MARK A.J. CHAPLAIN‡

Abstract. The ability to locally degrade the *extracellular matrix* (ECM) and interact with the tumour microenvironment is a key process distinguishing cancer cells from normal cells, and is a critical step in the metastatic spread of the tumour. The invasion of the surrounding tissue involves the coordinated action of the cancer cells, the ECM, the *matrix degrading enzymes*, and the *epithelial-to-mesenchymal transition*. In this paper, we present a mathematical model which describes the transition from an epithelial invasion strategy of the *epithelial-like cells* (ECs) to an individual invasion strategy for the *mesenchymal-like cells* (MCs). We achieve this by formulating a genuinely multiscale and hybrid system consisting of *partial* and *stochastic differential equations* that describe the evolution of the ECs and the MCs while accounting for the transitions between them. This approach allows one to reproduce, in a very natural way, fundamental qualitative features, of the current biomedical understanding of cancer invasion, that are not easily captured by classical modelling approaches, for example, the invasion of the ECM by self-generated gradients and the formation of EC invasion islands outside of the main body of the tumour.

Key words. Cancer invasion, multiscale modelling, hybrid continuum-discrete, coupled partial and stochastic partial differential equations

AMS subject classifications. 92B05, 92C17, 60H15, 35M30

1. Introduction.

Identified as one of the *hallmarks of cancer*, Hanahan and Weinberg [2000, 2011], cancer invasion is a complex process involving numerous interactions between the cancer cells and the *extracellular matrix* (ECM) (the tumour *microenvironment*) facilitated by matrix degrading enzymes. By its nature, the invasion involves the development and alteration of the cell-cell and cell-matrix adhesion processes. Broadly speaking, during the progression to full malignancy, cancer cells reduce their cell-cell adhesions and gain cell-matrix adhesions. Coupled with changes in the cell migration and proliferation, this enables the local spread of cancer cells into the surrounding tissue. Any encounter with blood or lymphatic vessels in the tumour microenvironment initiates the spread of the cancer to secondary locations in the host organism i.e. metastasis, Mehlen and Puisieux [2006], Weigelt et al. [2005].

Having been studied in some detail for the past 15-20 years, it has become clear that cancer invasion has a certain degree of diversity in its migratory mechanisms and of plasticity in cellular behaviour and properties. The diversity of cancer invasion mechanisms is illustrated schematically in Fig. 1 and their behavioural plasticity in Fig. 2. Both types of invasion are extensively discussed in Friedl and Wolf [2003]. Subsequently, cancer invasion can be broadly classified into two main groups, differing in the behaviour of how the cells migrate—individually or collectively—and how

* Mathematical Institute, School of Mathematics and Statistics, University of St. Andrews, St. Andrews KY16 9SS, Scotland, UK and Institute of Applied Mathematics, Faculty of Mathematics and Informatics, Heidelberg University, Heidelberg 69120, Germany n.sfakianakis@st-andrews.ac.uk

† Department of Mathematics, School of Mathematical and Physical Sciences, University of Sussex, Brighton BN1 9QH, UK and Department of Mathematics, University of Johannesburg, South Africa A.Madzvamuse@sussex.ac.uk

‡ Mathematical Institute, School of Mathematics and Statistics, University of St Andrews, St Andrews KY16 9SS, Scotland, UK majc@st-andrews.ac.uk

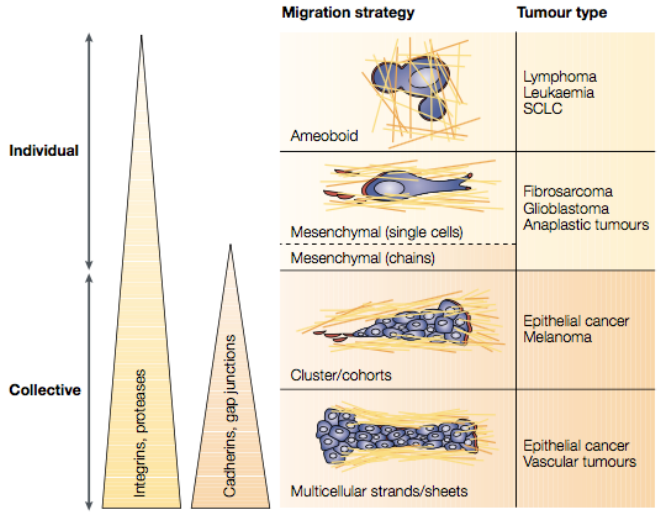

FIG. 1. *"Diversity of cancer invasion". Classification of the various migration and invasion strategies and corresponding types of tumour. As the complexity of the tumour increases, so do the expressions of cell-matrix and cell-adhesion molecules (integrins and cadherins) and the characterisation of the invasion as individual or collective. Figure adopted from Friedl and Wolf [2003]. (PERMISSION REQUESTED)*

these are controlled by different intra-cellular molecular programmes. Accordingly, cancer invasion can be characterised as *epithelial* or *collective invasion* whereby clusters or sheets of connected cells move en masse, or as *mesenchymal* or *individual invasion* whereby single cancer cells or small numbers of cancer cells actively invade the microenvironment.

Cancer cells may transition back and forth between the two mechanisms during the invasion process as they penetrate the surrounding tissue. The transition from *epithelial* to *mesenchymal invasion* is known as the *epithelial-to-mesenchymal transition* (EMT), and the opposite as *mesenchymal-to-epithelial transition* (MET). Both the EMT and MET processes are largely controlled by variations in the expression levels of *integrins*, *proteases*, and *cadherins* and varying cell-cell communication via *gap junctions*. They are moreover induced by, e.g., the secreted *transforming growth factor beta* (TGF-β) and the *epidermal growth factor* (EGF) proteins. We refer the reader to consult Thiery [2002], Roche [2018], Kalluri and Weinberg [2009], Te Boekhorst et al. [2016], and the references therein for detailed discussions on the triggering of EMT; MET; and their properties and role in development and cancer.

An alternative invasion mechanism, known as *amoeboid invasion* also exists, whereby individual cells exhibit morphological plasticity and develop the ability to squeeze through gaps in the ECM, rather than modify/degrade the ECM via matrix degrading enzymes, e.g. *urokinase-type plasminogen activator* (uPA), and matrix degrading *metalloproteases* (MMPs), Madsen and Sahai [2010], Sabeh et al. [2009].

Cancer invasion has also been the focus of mathematical modelling over the past twenty years or so, beginning with the work of Gatenby and Gawlinski [1996]. Since then, many different models and approaches have been formulated, some taking an

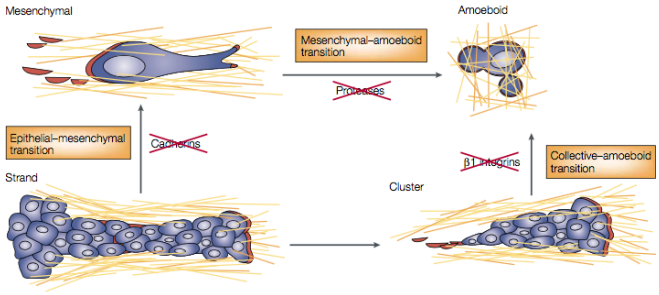

FIG. 2. *"Plasticity of cancer invasion". The character of cancer cell migration changes from collective to individual, following the loss of the cadherin or β1 integrin function. The corresponding cellular transition programmes are conditionally reversible, leading to metastases at later locations within the organism. Figure from Friedl and Wolf [2003].* *(PERMISSION REQUESTED)*

individual-based approach e.g. Ramis-Conde et al. [2008a,b], Hatzikirou et al. [2010], Wang et al. [2013], Schlüter et al. [2015], others adopting a continuum approach using systems of partial differential equations e.g. Chaplain and Orme [1996], Preziosi [2003], Chaplain and Lolas [2005, 2006], Andasari et al. [2011], Domschke et al. [2014a], Deakin and Chaplain [2013], Painter and Hillen [2013], Kolbe et al. [2016], Sfakianakis et al. [2017], Engwer et al. [2017], Peng et al. [2017], while others have adopted a hybrid continuum-discrete approach, e.g. Anderson et al. [2000], Anderson [2005], Colombi et al. [2017]. An individual-based approach has the advantage of being able to focus on single cells, account for cellular processes in detail, and is more accurate at smaller scales and smaller cell numbers. On the other hand, the averaging of the microscale dynamics that takes place in the continuum approach has the advantage of being able to capture macroscopic processes and efficiently model large scales without having to resort to high performance computing. Moreover, the continuum approach has the added benefit to allow for mathematical analysis of the developed models.

In the current paper, we apply a *multiscale modelling framework* to cancer invasion that explicitly incorporates the transition from epithelial to individual invasion and vice versa. In particular, we describe the *epithelial-like cancer cells* (ECs) through a *density distribution* and their spatiotemporal evolution by a *macroscopic deterministic model*. On the other hand, the *mesenchymal-like cancer cells* (MCs) are modelled by an *atomistic* approach, and their spatiotemporal evolution by an *individual stochastic model*. This is a genuinely *hybrid* approach where we explicitly include the EMT and MET processes between the two cancer cell types and their corresponding discrete and continuum descriptions.

Previous approaches in the literature of a similar modelling philosophy and scientific focus are not many. We refer for instance to the works of Colombi et al. [2015a,b], where the authors employ a measure theoretic approach to study cell differentiation and aggregation, to Colombi et al. [2017] in which a biological and mathematical "switch" between a concentrated cell-particle description and the corresponding distributed mass approach is studied, to Capasso and Morale [2010] where a "doubly stochastic" system of interacting cell-particles is studied leading, in the large cell-particle limit, to deterministic *partial differential equations* (PDEs), Hiremath and Surulescu [2016a], Hiremath et al. [2018], Colombi and Scianna [2017] where coupled PDE-SDE (*stochastic differential equations*) systems describing biological processes

at population, cellular, and sub-cellular scales are studied, and to Cañizo et al. [2015], Carrillo et al. [2018] where continuum models of (energy) interacting cell-particles are studied and the existence of global minimizers is established.

2. Model derivation. The modelling framework that we propose is a genuinely hybrid combination of the two cancer cell types, ECs and MCs, described by a continuum density and a collection of discrete cells. For the sake of clarity of presentation, the development of the model and the corresponding techniques are constrained to the two (spatial) dimensional case.

Therefore, our paper is structured as follows. In Section 2.1 we describe the *continuum density submodel* of the problem. This is a macroscopic deterministic model that addresses the spatiotemporal evolution of the densities of the ECs, ECM, and the MMPs. In this submodel, the MCs participate only implicitly, i.e. they influence the ECs and the rest of the components of the submodel but their time evolution is not dictated by it. We then introduce the *discrete cell-particle* submodel of the problem in Section 2.2. This submodel describes the time evolution of the MC cells, including their biased random motion along the gradients of the ECM. It does not include cell growth or proliferation although they can be easily incorporated in the model. The coupling between the continuum components (ECs, ECM, MMPs) and the discrete (MCs) occurs in several places: the proliferation of the ECs, the degradation of the ECM, the production of the MMPs, the haptotaxis of the MCs, and most notably the transition between the ECs and MCs. In particular, in Section 2.3 we describe the transitions between the density and cell-particle phases of the cancer cells. We address the way the MC cells are "substantiated" from their density formulation via a *density-to-particle* process, and how they transition back to density via an opposite *particle-to-density* process. In Section 2.4 we present the combined spatiotemporal evolution of the two cancer cell types under the prism of the EMT and MET processes.

2.1. Density formulation. From a *macroscopic deterministic* approach, we follow the seminal works of Liotta et al. [1977], Gatenby and Gawlinski [1996], Anderson et al. [2000], Byrne et al. [1999] and describe the ECs, MMPs, and ECM by their densities. The MCs are primarily described as isolated cell-particles; the model for their time evolution is derived in Section 2.2. It should be noted that the MCs appear also in the density formulation as they directly affect the ECs, MMPs, and the ECM. Since the focus of this paper is on the combination of the two cancer cell phenotypes and their corresponding discrete and continuum phases, rather than on the biological applications of the model, we incorporate only the very basic biological processes. More detailed and cancer-type specific models will be considered in follow up works.

Indeed, we mainly assume that the ECs are transformed to MCs and vice-versa via the MET and EMT processes, and that they proliferate by following a *logistic volume-filling* constraint as they compete for free space and resources with each other, the MCs and the ECM. Furthermore, we assume that the ECs diffuse in the environment; although this process is expected to be very slow. This is included in the model to capture, in a simplified and linear way the effect of mechanical forces exerted on the cells. More realistic assumptions of the diffusion can be considered by accounting for the appropriate biological phenomena and extending the model accordingly. The same holds true for the -taxis driven migration as well; extensions of the model can account for a plethora of intra- and extra-cellular processes relevant to the migration of cancer cells.

To proceed, we denote by $\Omega \subset \mathbb{R}^2$ the Lipschitz domain of study, and by $c^\alpha(\mathbf{x},t)$, $c^\beta(\mathbf{x},t)$, $m(\mathbf{x},t)$, and $v(\mathbf{x},t)$, $\mathbf{x}\in\Omega$ and $t\geq 0$ the densities of the ECs, MCs, MMPs, and the ECM respectively. From here onwards, we denote by superscripts α and β the two types of cancer cells, the ECs and MCs, respectively.

Based on the above discussions, we consider the following equation for the evolution of the ECs

$$\begin{aligned}\frac{\partial}{\partial t}c^\alpha(\mathbf{x},t) = \underbrace{D_\alpha \Delta c^\alpha(\mathbf{x},t)}_{\text{diffusion}} - \underbrace{\mu_\alpha^{\text{EMT}}(\mathbf{x},t)c^\alpha(\mathbf{x},t)}_{\text{EMT}} + \underbrace{\mu_\beta^{\text{MET}}(\mathbf{x},t)c^\beta(\mathbf{x},t)}_{\text{MET}} \\ + \underbrace{\rho_c^\alpha c^\alpha(\mathbf{x},t)\left(1-c^\alpha(\mathbf{x},t)-c^\beta(\mathbf{x},t)-v(\mathbf{x},t)\right)}_{\text{proliferation}},\end{aligned} \tag{1a}$$

where $\mu_\alpha^{\text{EMT}}(\mathbf{x},t) = \mu_\alpha \mathcal{X}_{\mathcal{E}(t)}(\mathbf{x})$, $\mu_\beta^{\text{MET}}(\mathbf{x},t) = \mu_\beta \mathcal{X}_{\mathcal{M}(t)}(\mathbf{x})$, with $\mathcal{E}(t), \mathcal{M}(t) \subset \Omega$, and $D_\alpha,\ \mu_\alpha,\ \mu_\beta, \rho_c^\alpha \geq 0$.

As previously noted, the MCs are described by their cell-particle formulation —which we present in Section 2.2— and the corresponding evolutionary equations. The MCs participate in (1a) via their density c^β after having undergone a specific *particle-to-density* transformation; this is discussed in Section 2.3.

Since the triggering mechanisms of EMT and MET are not the focus of this work, we refrain from a detailed modelling. We instead assume a simplified approach where EMT occurs in a randomly chosen subset of the domain $\mathcal{E}(t) \subset \Omega$ in (1a). We understand $\mathcal{E}(t)$ as the union of a number of sets each having the size of a single biological cell, cf. (11) and Section 2.3 for further discussion on the way that $\mathcal{E}(t)$ is formed. In a similar way, we assume that the MET occurs randomly at every cell-particle each giving rise to a domain of the size of a biological cell, and their union to the set $\mathcal{M}(t)$; see also (16) and Sections 2.2 and 2.3 for further details.

We also assume that both types of cancer cells, ECs and MCs, produce MMPs, which in turn diffuse in the environment (molecular diffusion) and decay with a constant rate, thus satisfy:

$$\frac{\partial}{\partial t}m(\mathbf{x},t) = \underbrace{D_m \Delta m(\mathbf{x},t)}_{\text{diffusion}} + \underbrace{\rho_m^\alpha c^\alpha(\mathbf{x},t) + \rho_m^\beta c^\beta(\mathbf{x},t)}_{\text{production}} - \underbrace{\lambda_m m(\mathbf{x},t)}_{\text{decay}}, \tag{1b}$$

with $D_m,\ \rho_m^\alpha,\ \rho_m^\beta,\ \lambda_m \geq 0$ constants. Alternative approaches could also be considered, e.g. an ECM-density dependent production of the MMPs by the cancer cells.

We assume that the ECM is represented by the density of the *collagen macromolecules*, and is therefore modelled as a non-uniform, immovable component of the system that neither diffuses nor otherwise translocates. Furthermore, we assume that the ECM is degraded by the combined action of the cancer cells/MMPs complex. Finally, for simplicity, no reconstruction of the matrix is assumed. Overall, the evolution equation of the ECM is given by

$$\frac{\partial}{\partial t}v(\mathbf{x},t) = -\underbrace{\left(\lambda_v^\alpha c^\alpha(\mathbf{x},t) + \lambda_v^\beta c^\beta(\mathbf{x},t)\right) m(\mathbf{x},t)v(\mathbf{x},t)}_{\text{degradation}}, \tag{1c}$$

with $\lambda_v^\alpha,\ \lambda_v^\beta \geq 0$ constants. We are motivated by Sabeh et al. [2009], to model the matrix degradation in this particular way, i.e. dependent on the complex cancer

cells/MMPs instead of the MMPs alone. Possible extensions of the model could include non-diffusible MMPs, MC-only matrix degradation, matrix reconstruction, and other biologically relevant processes.

The *(advection-)reaction-diffusion*[1] (A-)RD system (1a)–(1c) can also be written in a more convenient matrix-vector compact form for the numerical treatment formulation, see also Appendix A. In particular, using the notation

$$\mathbf{w}(\mathbf{x},t) = \left(c^{\alpha}(\mathbf{x},t), m(\mathbf{x},t), v(\mathbf{x},t)\right)^{T},$$

(1a)–(1c) read

$$\mathbf{w}_t(\mathbf{x},t) = D(\mathbf{w}(\mathbf{x},t)) + R(\mathbf{w}(\mathbf{x},t)), \tag{2}$$

where

$$D(\mathbf{w}) = \mathbb{D}\Delta\mathbf{w} \text{ and } R(\mathbf{w}) = \begin{pmatrix} -\mu_{\alpha}^{\mathrm{EMT}} c^{\alpha} + \mu_{\beta}^{\mathrm{MET}} c^{\beta} + \rho_{c}^{\alpha} c^{\alpha}\left(1 - c^{\alpha} - c^{\beta} - v\right) \\ \rho_{m}^{\alpha} c^{\alpha} + \rho_{m}^{\beta} c^{\beta} - \lambda_{m} m \\ -\left(\lambda_{v}^{\alpha} c^{\alpha} + \lambda_{v}^{\beta} c^{\beta}\right) m v \end{pmatrix},$$

with $\mathbb{D} = diag(D_{\alpha}, D_{m}, 0)^{T}$, denote the *diffusion* and *reaction* operators, respectively. As noted previously, in the more general case where chemotaxis or haptotaxis are considered, the corresponding formulation should also include an *advection* operator.

Clearly, cancer invasion models of the form (2) are mere simplifications of the biological reality; they are also quite simple in their mathematical structure. Still their analytical and numerical investigations are challenging; depending on the actual structure of the assumed model, whether e.g. -taxis, non-local adhesion, or non-linear diffusion is included in (2). Indicatively, we refer to Hillen et al. [2017], Marciniak-Czochra and Ptashnyk [2010], Andasari et al. [2011], Giesselmann et al. [2018], Stinner et al. [2016], Kolbe et al. [2016], Marciniak-Czochra et al. [2013], Winkler and Tao [2014] and the references therein, for the study of a various cases of cancer invasion models. One of the reasons for this, is their mixed nature, i.e. the ECs and MMPs obey *partial differential equations* (PDEs) with respect to time and space, whereas the ECM obeys an *ordinary differential equation* (ODE) with respect to time for every point in space.

2.2. Particle formulation. We are motivated in this description by methods and techniques that have been used previously in other scientific fields. One such example is the classical *particle-in-cell* (PIC) method which was first proposed in Harlow [1965] and used among others in plasma physics. A second example is the *smoothed-particle hydrodynamics* (SPH) method used in astrophysics and ballistics see e.g. Gingold and Monaghan [1977]. The stochastic nature of the ODEs that the cell-particles obey is motivated by the seminal work of Stratonovich [1966]. For the combination of the two cancer cell formulations, we are inspired by Blanc et al. [2007], Kitanidis [1994], Makridakis et al. [2014], Tompson and Dougherty [1992].

In view of the above, we describe the MCs as a system of N cell-particles that are indexed by $p \in P = \{1, \ldots, N\}$, and account for their positions $\mathbf{x}_p(t) \in \mathbb{R}^2$ and masses $m_p(t) \geq 0$. We allow for their number to vary in time and so we set $N = N(t) \in \mathbb{N}$.

[1] In the general case, the ECs equation (1a) could include -taxis terms in the form of advection as well.

The mass distribution of such a system of cell-particles, $\{(\mathbf{x}_p, m_p),\ p \in P\}$, is given by

$$\tilde{\tilde{c}}(\mathbf{x}, t) = \sum_{p \in P} m_p(t)\delta(\mathbf{x} - \mathbf{x}_p(t)), \tag{3}$$

where $\delta(\cdot - \mathbf{x}_p(t))$ represents the Dirac distribution centred at $\mathbf{x}_p \in \mathbb{R}^2$. Clearly (3) is not a function so we consider a *kernel* ζ and re-define the *mass distribution* of the cell-particles $\{(\mathbf{x}_p, m_p),\ p \in P\}$ as

$$\tilde{c}(\mathbf{x}, t) = \int_\Omega \tilde{\tilde{c}}(\mathbf{x}', t)\zeta(\mathbf{x} - \mathbf{x}')d\mathbf{x}' \overset{(3)}{=} \sum_{p \in P} m_p(t)\zeta(\mathbf{x} - \mathbf{x}_p(t)). \tag{4}$$

The function ζ need not be smooth; to simplify hence the rest of this work we choose the characteristic function of the rectangle K_0 *centred* at the origin $\mathbf{0} \in \mathbb{R}^2$

$$\zeta(\mathbf{x}) = \mathcal{X}_{K_0}(\mathbf{x}), \quad \mathbf{x} \in \mathbb{R}^2. \tag{5}$$

The choice of K_0 (shape, size, and location) is justified in Sections 2.2.1 and 3.

2.2.1. Interactions between cell-particles. We understand the cell-particles as isolated cancer cells or cancer-cell aggregates of similar size and masses. To maintain though similar masses, we split and merge the cell-particles according to their mass and position. In particular, when a cell-particle represents an isolated cancer cell, we set m_{ref} to be the reference cell mass and K_0 its (two-dimensional) footprint, and proceed as follows:

Splitting. A cell-particle $(\mathbf{x}_p, m_p)$ with mass $m_p > \frac{4}{3}\, m_{\text{ref}}$ is *split* into two cell-particles $(\mathbf{x}_p^1, m_p^1)$, $(\mathbf{x}_p^2, m_p^2)$ of the same position $\mathbf{x}_p^1 = \mathbf{x}_p^2 = \mathbf{x}_p$ and mass $m_p^1 = m_p^2 = \frac{1}{2}\, m_p$. From that moment onwards, these two cell-particles are considered different from each other.

Merging. A *small cell-particle* $(\mathbf{x}_p, m_p)$ with mass $m_p < \frac{2}{3}\, m_{\text{ref}}$ is *merged* with another small cell-particle $(\mathbf{x}_q, m_q)$ if they are close to each other i.e.

$$\|\mathbf{x}_p - \mathbf{x}_q\| < \operatorname{diam}(K_0),$$

where $\|\cdot\|$ describes the two-dimensional Euclidean norm. The resulting cell-particle is set to have the cumulative mass of the two cell-particles and to be located at their (intermediate) centre of mass

$$\left(\frac{m_p\mathbf{x}_p + m_q\mathbf{x}_q}{m_p + m_q}, m_p + m_q\right). \tag{6}$$

If more than two small cell-particles are found in merging distance at the same time, they are merged pair-wise in the order they have been created.

Given that the distance between the cell-particles is sufficiently small, iterations of the *merging* and *splitting* processes lead to cell-particles with masses $m_p \in [\frac{2}{3}\, m_{\text{ref}}, \frac{4}{3}\, m_{\text{ref}}]$, i.e. cell-particles with more-or-less the reference cell mass m_{ref}.

These two processes are primarily meant to deal with two particular biological phenomena: the formation of MC-clusters and the cell growth and mitosis. Still, as the

focus of the current paper is more methodological, and since we respect a go-or-grow dichotomy between the ECs and the MCs, we postpone the discussion of the underlying biological procedures and the corresponding mathematical modelling to a future work. Besides the merging and splitting procedures, we do not consider other processes that alter the masses of the cell-particles. We also do not consider any further interactions between the cell-particles in this work (such as competition for free space or development of collision forces) as we try to be consistent with the dynamics that are usually assumed by macroscopic deterministic models similar to (1a)–(1c). In effect, two or more cell-particles could occupy the same physical position, in the same way as the local density of cancer cells can be large.

2.2.2. Time evolution of cell-particles. We assume that the cell-particles perform a *biased random motion* that is comprised of two independent processes: a *directed-motion* part that represents the *haptotactic* response of the cells to gradients of the ECM-bound adhesion sites, and a *random/stochastic-motion* part that describes the undirected *kinesis* of the cells as they sense the surrounding environment; we understand this phenomenon as a *Brownian motion*. We reproduce this way, at the cell-particle level, the diffusion and -taxis dynamics prescribed by the *macroscopic deterministic* cancer invasion models, see e.g. Anderson et al. [2000].

In a slightly more general framework, we assume that the cell-particles obey a *stochastic differential equation* (SDE) of the (differential) form

$$d\mathbf{X}_t^p = \mu\left(\mathbf{X}_t^p, t\right) dt + \sigma\left(\mathbf{X}_t^p, t\right) d\mathbf{W}_t^p, \quad \text{for } p \in P, \tag{7a}$$

where $\mathbf{X}_t^p$ represents the position vector of the cell-particles $p \in P$ and $\mathbf{W}_t^p$ is a Wiener process with independent components. Here, μ and σ^2 are the *drift* and *diffusion* coefficients that encode the modelling assumptions made on the directed and random parts of the motion of the cell-particles. Their contribution in (7a) can be understood as follows: during a short time period δt the changes of the stochastic process $\mathbf{X}_t^p$ follow a normal distribution with expectation $\mu\left(\mathbf{X}_t^p, t\right)\delta t$ and variance $\sigma\left(\mathbf{X}_t^p, t\right)^2 \delta t$. Further insight into (7a) can be heuristically derived from the corresponding *random equation*

$$\frac{d}{dt}\mathbf{X}_t^p = \mu\left(\mathbf{X}_t^p, t\right) + \sigma\left(\mathbf{X}_t^p, t\right)\xi_t^p, \quad \text{for } p \in P, \tag{7b}$$

where the integral of the *noise* ξ_t^p gives rise to the Wiener process $\mathbf{W}_t^p$. The noise ξ_t^p along with the intensity σ represent the fluctuations around the expected value of the velocity μ. In the current work, and primarily for the sake of simplicity, we assume that μ depends on the gradient of the ECM and σ is constant. If more complex dynamics and, most notably, if interactions between the cell-particles and/or the environment are assumed, μ and σ should be adjusted accordingly.

We do not undertake an analysis of (7a) here. However, we note that it should be performed over a complete probability space $(\mathcal{S}, \mathcal{H}, \mathbb{P})$ with a filtration $\{\mathcal{H}_t\}_{t\geq 0}$. The sample space $\mathcal{S}$ can be seen as containing all cell-particles ω belonging to one particular tumour. Thus, for every $p \in P$, the position vector $\mathbf{X}^p : S \times [0,\infty) \to \mathbb{R}^2$ represents an appropriate stochastic process. For more details, we refer to, eg., Oksendal [2003].

Furthermore, in the special case $\mu(\mathbf{x}, t) = \alpha\mathbf{x}$ and $\sigma(\mathbf{x}, t) = \beta$, $\alpha \in \mathbb{R}$ and $\beta \geq 0$, the stochastic process that solves (7a) can be numerically approximated by the corresponding *half-step explicit Euler-Maruyama particle motion scheme*,

$$\mathbf{X}_{t+\tau}^p = \mathbf{X}_t^p + \alpha\mathbf{X}_t^p\tau + \beta\mathbf{Z}^p\sqrt{\tau}, \quad \text{for} \quad p \in P\,, \tag{7c}$$

with $\tau > 0$ being the timestep of the scheme, and $\mathbf{Z}^p$ a vector of normally distributed values of zero mean and unit variance, c.f. Appendix B and Kloeden and Platen [1992].

Although not the aim of the current work, we note that the many-particle limit $N \to \infty$ in (7a) is important as it allows to recover the macroscopic deterministic equation that the MCs would satisfy, if the $N \to \infty$ limit was relevant and justified. In the special case of (7c) the $N \to \infty$ limit would give rise to an advection-diffusion equation for the corresponding densities, with constant diffusion coefficient $\frac{1}{2}\beta^2$ and non-constant advection speed $\alpha\mathbf{x}$, see e.g. Kitanidis [1994], Tompson and Dougherty [1992], Stratonovich [1966]. Conversely, if the diffusion coefficient of the macroscopic equation is non-constant as, e.g., in Engwer et al. [2017] the corresponding particle-motion scheme should read, instead of (7c), as

$$\mathbf{X}^p_{t+\tau} = \mathbf{X}^p_t + \mathbf{A}(\mathbf{X}^p_t)\tau + \mathbf{B}(\mathbf{X}^p_t) \cdot \mathbf{Z}^p\sqrt{\tau}, \quad \text{for} \quad p \in P\,, \tag{8}$$

with the *advection operator*

$$\mathbf{A} = \mathbf{v} + \nabla \cdot \mathbf{D}, \tag{9}$$

encoding the *advection speed* $\mathbf{v}$ of the macroscopic equation adjusted by a *drift term* that involves the diffusion matrix $\mathbf{D}$, and where

$$\mathbf{B} \cdot \mathbf{B}^T = 2\mathbf{D}. \tag{10}$$

If $\mathbf{v}$ and $\mathbf{D}$ depend on the physical space, the Itô-type correction of the advection speed $\mathbf{v}$ in (9) is necessary so that the many-particle limit $N \to \infty$ of (8) converges to the correct macroscopic equation. We refer to Arnold [1974], Raviart [1986], Stratonovich [1966], Tompson and Dougherty [1992] and Kitanidis [1994] for further discussions and proofs of these claims.

Modelling reactions. Although the MCs participate in several reaction processes (such as the EMT, MET, the proliferation of the ECs, the production of MMPs, and the degradation of the ECM), the particle motion scheme (8) does not include any reaction terms. We account for them in the following way:

Some of the MC cell-particles undergo MET to ECs, and subsequently are transformed to density via the *particle-to-density* operator that will be introduced in Section 2.3. These MCs are removed from the system of the MC cell-particles. The new EC density is added to the existing one and participates normally in the system (1a)–(1c). Conversely, a part of the EC density undergoes EMT towards MC, at first as density, which is then transformed into cell-particles via a *density-to-particle* operator defined in Section 2.3. These newly formed MCs are then added to the system of the existing MC cell-particles.

We also note that within this framework, the modelling of cell-growth (increase of cellular mass) and cell-mitosis are straight forward. Still, as we respect, in the current paper, a go-or-grow dichotomy between the ECs and MCs, we do not study these processes any further.

Moreover, at every timestep of the method, the full distribution of MC cell-particles is transformed temporarily to density (without undergoing MET to ECs), via the *particle-to-density* operator. They participate then in the proliferation of the ECs, the production of the MMPs, and the degradation on the ECM, cf. (1a)–(1c). We give more details on the combination of the ECs and MCs in Section 2.4.

2.3. Modelling phase transitions between cell-particles and densities. In this section we describe the *particle-to-density* and the *density-to-particle* phase transition operators.

We assume at first, that the domain Ω is regular (e.g. rectangle in two-dimensions) and large enough (of the order of 10^2–10^4 biological cells), to be *uniformly partitioned* in equal rectangles/*partition cells* $\{M_i, i \in I\}$

$$\Omega = \bigcup_{i \in I} M_i, \tag{11}$$

where every M_i is an affine translation of the *generator cell* K_0. Note that K_0 is the same as the support of the characteristic function in (5). Clearly $|M_i| = |K_0| = K > 0$.

Remark 2.1. *More general domains Ω can also be considered, possibly at the expense of the equality of the M_is and the upcoming mass distribution relations (16), (18). Note moreover that the partition cells M_i, $i \in I$ do not coincide with the discretisation cells of the numerical method used to solve (1a)–(1c). The latter constitute an instance of a sequence of computational grids of zero-converging step sizes, whereas the former have a step size that represents physical properties of biological cells and remains fixed over all computational grid resolutions.*

Using the partitioning of Ω to $\{M_i, i \in I\}$, we represent a measurable $c : \Omega \times (0, \infty) \to \mathbb{R}$ by its *simple-function* decomposition

$$\sum_{i \in I} c_i(t) \mathcal{X}_{M_i}(\mathbf{x}), \tag{12}$$

where $\mathcal{X}_{M_i}$ is the characteristic function of the set $M_i \subset \Omega$, and $c_i(t)$ the mean value of $c(\cdot, t)$ over M_i

$$c_i(t) = \frac{1}{K} \int_{M_i} c(\mathbf{x}, t) d\mathbf{x}. \tag{13}$$

Clearly, this representation conserves the mass of $c(\cdot, t)$ over Ω

$$\sum_{i \in I} K c_i(t) = \int_{\Omega} c(\mathbf{x}, t) d\mathbf{x} \tag{14}$$

On the other hand a particle, indexed here by $p \in P$, can be represented either by its position and mass (*particle formulation*)

$$(\mathbf{x}_p(t),\, m_p(t))\,, \tag{15}$$

or by the characteristic function with density value (*density formulation*)

$$\frac{m_p(t)}{K} \mathcal{X}_{K_p}(\mathbf{x}), \tag{16}$$

where K_p is the affine translation of the generator cell K_0 and is centred at $\mathbf{x}_p$. Clearly (16) implies that the mass m_p of the particle is uniformly distributed over K_p.

Although the K_p, $p \in P$ and the M_i, $i \in I$ in (12) are equivalent up to affine translations (to the K_0), they do not in general coincide. The M_i, $i \in I$ form a fixed partition of the domain, cf. (11), whereas the K_p, $p \in P$ follow the position of the cell-particles (16).

Based on the dual description (15) and (16) of the cell-particles, we set forth the *transition operators* between cell-particles and densities.

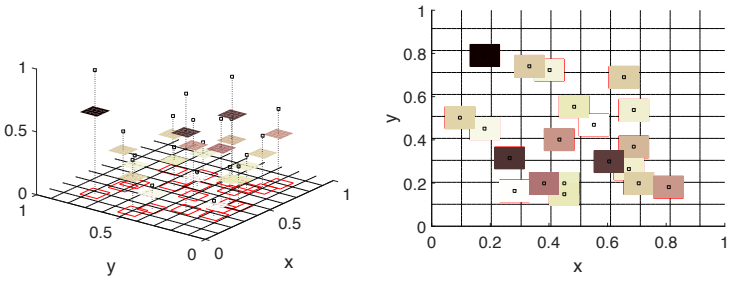

FIG. 3. *Two-dimensional graphic representation of the particle-to-density operator $\mathcal{F}$. (left:) We consider a support K_p ($p \in P$) around the location x_p of every particle. The mass of every particle m_p, (shown as points) is uniformly distributed over the respective support K_p. The grid represents the partitioning of the domain. (right:) A view from above reveals that the supports K_p can overlap with several cells of the partition. The corresponding masses are assigned to the partition cells using (19).*

2.3.1. Particles-to-density transition. Let $\{(\mathbf{x}_p(t), m_p(t)),\ p \in P\}$ be a collection of cell-particles. Using (4), we define the *particle-to-density* operator $\mathcal{F}$ as,

$$\{(\mathbf{x}_p(t), m_p(t)),\ p \in P\} \xrightarrow{\mathcal{F}} c(\mathbf{x}, t). \tag{17}$$

To define the target function $c(\mathbf{x}, t)$, we go through all the cell-particles, indexed here by $p \in P$, and consider their corresponding density formulation (16). The support K_p of the cell-particles, overlaps with (possibly) several[2] of the partition cells M_i, $i \in I$. In each of these partition cells, and in view of (16), we assign the corresponding portion of the particle mass

$$m_p\big|_{M_i} = \frac{m_p}{K}\big|K_p \cap M_i\big|. \tag{18}$$

Due to the simple-function decomposition (12)–(13), we account for the contribution of all cell-particles $p \in P$ to the partition cell M_i by

$$c_i(t) = \sum_{p \in P} \frac{1}{K} m_p\big|_{M_i} \overset{(18)}{=} \sum_{p \in P} \frac{m_p(t)}{K^2}\big|K_p \cap M_i\big|, \qquad \text{for } i \in I\,. \tag{19}$$

In view now of (12) and (19), we deduce the density function $c(\mathbf{x}, t)$ (as a simple function) over the full domain Ω as

$$c(\mathbf{x}, t) = \sum_{i \in I} c_i(t)\mathcal{X}_{M_i}(\mathbf{x}), \quad \mathbf{x} \in \Omega. \tag{20}$$

Refer to Fig. 3 for a graphical representation of the *particle-to-density* operator $\mathcal{F}$ in two dimensions.

2.3.2. Density-to-particles transition. Conversely, we define the *density-to-particle operator* $\mathcal{B}$ for a given density function $c(\mathbf{x}, t)$ by

$$\{(\mathbf{x}_p(t), m_p(t)),\ p \in P\} \xleftarrow{\mathcal{B}} c(\mathbf{x}, t), \tag{21}$$

[2]Since the sets K_p, $p \in P$ and M_i, $i \in I$ are two-dimensional quadrilaterals of the same dimensions, every K_p overlaps with at most five M_is.

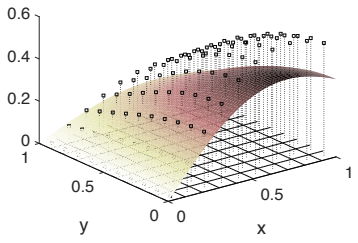

FIG. 4. *Graphical representation of the density-to-particle operator $\mathcal{B}$. We compute the mass m_i of the density function $c(\mathbf{x},t)$ (surface), over every partition cell M_i, $i \in I$ (quadrilateral grid on the xy plane), using (22). We then define the particle as $(\mathbf{x}_i, m_i)$ where the location $\mathbf{x}_i$ is given by (23).*

in the following way: in every partition cell M_i, $i \in I$, we assign one particle with mass

$$m_i(t) = \int_{M_i} c(\mathbf{x},t)d\mathbf{x}, \tag{22}$$

and position

$$\mathbf{x}_i(t) = \text{ the (bary)centre of } M_i. \tag{23}$$

For practical considerations, we set in the numerical simulations a minimum threshold value on the densities, below which no transition to cell-particles takes place. This threshold value is quite small and is used to avoid large numbers of cell-particles of negligible mass. Refer to Fig. 4 for a graphical representation of the *density-to-particles* operator.

2.4. Coupling of the two cancer cell phenotypes and phases. We denote again the two cancer cell phenotypes, EC and MC, by the superscripts α and β respectively, and consider for $t \geq 0$ the vector formulation (2) of the system (1a)–(1c) with the density variables

$$\mathbf{w}(\mathbf{x},t) = (c^\alpha(\mathbf{x},t), m(\mathbf{x},t), v(\mathbf{x},t)) .$$

At the same physical time t, we write the MC cell-particles as

$$\mathcal{P}^\beta(t) = \left\{ \left(\mathbf{x}_p^\beta(t), m_p^\beta\right), p \in P(t) \right\}, \tag{24}$$

and, accordingly, the overall system is given by the tuple

$$\left(\mathbf{w}(\mathbf{x},t), \mathcal{P}^\beta(t)\right), \ \mathbf{x} \in \Omega, \ t \geq 0. \tag{25}$$

In the evolution of the overall system, we consider the EMT and MET processes separately from the rest of the dynamics of the system (1a)–(1c)[3].

[3]To ease the presentation and since the EMT and MET are assumed to be *instantaneous* and *tautochronous*, we drop the dependence of the density variables and the cell-particles on $\mathbf{x}$ and/or t.

2.4.1. EMT operator. The detailed modelling and biophysical accuracy of the EMT triggering mechanism is not one of the main focal points of this work. Instead, we assume a simplified approach where a randomly chosen part of the ECs (in density formulation) $c^{\alpha}_{\mathrm{EMT}}$ undergoes EMT to give rise to MCs (still in density formulation)

$$c^{\alpha}_{\mathrm{EMT}} \xrightarrow{\mathrm{EMT}} c^{\beta}_{\mathrm{EMT}}.$$

The newly created MC density c^{β}_{EMT} is transformed to MC cell-particles via the *density-to-particle* operator $\mathcal{B}$ given in (21)

$$c^{\beta}_{\mathrm{EMT}} \xrightarrow{\mathcal{B}} \left\{(\mathbf{x}^{\beta}_p, m^{\beta}_p),\ p \in P^{\mathrm{EMT}}\right\}, \tag{26}$$

where $\mathbf{x}^{\beta}_p$, m^{β}_p follow from (22), (23) and P^{EMT} is the corresponding set of indices. Subsequently, the family of existing MC cell-particles is updated with the newly created cell-particles. This is given by the disjoint union

$$\underbrace{\left\{(\mathbf{x}^{\beta}_p, m^{\beta}_p),\ p \in P\right\}}_{\text{existing MC cells}} \uplus \underbrace{\left\{(\mathbf{x}^{\beta}_p, m^{\beta}_p),\ p \in P^{\mathrm{EMT}}\right\}}_{\text{newly created MC cells}} = \left\{(\mathbf{x}^{\beta}_p, m^{\beta}_p),\ p \in P^{\mathrm{new}}\right\}, \tag{27}$$

where P^{new} is a re-enumeration of the multiset $P \uplus P^{\mathrm{EMT}}$.

Overall, combining the two cancer cell types, the EMT operator reads as

$$\mathcal{R}^{\mathrm{EMT}}\left(c^{\alpha}, \left\{\left(\mathbf{x}^{\beta}_p, m^{\beta}_p\right),\ p \in P\right\}\right) = \left(c^{\alpha} - c^{\alpha}_{\mathrm{EMT}}, \left\{(\mathbf{x}^{\beta}_p, m^{\beta}_p),\ p \in P^{\mathrm{new}}\right\}\right). \tag{28}$$

2.4.2. MET operator. As with the EMT, the triggering mechanism of the MET is not one of the focal points of this paper. We instead assume an approach where each of the MC cell-particles $\left\{\left(\mathbf{x}^{\beta}_p, m^{\beta}_p\right),\ p \in P\right\}$ undergoes MET to ECs randomly

$$\left\{(\mathbf{x}^{\beta}_p, m^{\beta}_p),\ p \in P\right\} \xrightarrow{\mathrm{MET}} \underbrace{\left\{(\mathbf{x}^{\alpha}_p, m^{\alpha}_p),\ p \in P^{\mathrm{MET}}\right\}}_{\text{newly created EC cells}}. \tag{29}$$

The resulting EC cell-particles are instantaneously transformed to density via the *particle-to-density* operator $\mathcal{F}$ given in (17):

$$\left\{(\mathbf{x}^{\alpha}_p, m^{\alpha}_p),\ p \in P^{\mathrm{MET}}\right\} \xrightarrow{\mathcal{F}} c^{\alpha}_{\mathrm{MET}}.$$

In operator form, the MET reads

$$\mathcal{R}^{\mathrm{MET}}\left(c^{\alpha}, \left\{\left(\mathbf{x}^{\beta}_p, m^{\beta}_p\right),\ p \in P\right\}\right) = \left(c^{\alpha} + c^{\alpha}_{\mathrm{MET}}, \left\{(\mathbf{x}^{\beta}_p, m^{\beta}_p),\ p \in \tilde{P}^{\mathrm{new}}\right\}\right), \tag{30}$$

where $\tilde{P}^{\mathrm{new}}$ is a re-enumeration of the set difference $P \setminus P^{\mathrm{MET}}$.

2.5. Time evolution of the two cancer cell types. The evolution of the ECs is controlled by (1a)–(1c) and through their coupling with the MCs cell-particles, by (7a). We study this combined system of PDEs and SDEs numerically while postponing any analytical investigations for a follow up work. To this end, we consider the model (2) and set

$$\begin{aligned}
\mathbf{W}^n &= \left\{\mathbf{w}^n_{(i,j)} = \left(c^n_{(i,j)}, m^n_{(i,j)}, v^n_{(i,j)}\right),\ (i,j) \in M_x \times M_y\right\},\\
\mathcal{P}^{\beta,n} &= \left\{\left(\mathbf{x}^{\beta,n}_p, m^{\beta}_p\right),\ p \in P^n\right\},
\end{aligned}$$

to denote numerical approximations of the density and particle variables $\mathbf{w}(\mathbf{x}, t)$ and $\mathcal{P}^\beta(t)$, respectively, at the instantaneous time $t = t^n$. Here, M_x, $M_y \in \mathbb{N}$ denote the resolution of the numerical grid along the x-, and y-directions respectively. We refer to the Appendix A for further information on the numerical method employed on $\mathbf{W}$; we focus here on the time evolution of the density and particle variables by means of an *operator splitting* approach. In particular, for $t \in [t^n, t^{n+1}]$, $t^{n+1} = t^n + \tau^n$, we assume that:

— During the time period $[t^n, t^n + \frac{1}{2}\tau^n]$, the system evolves, *without* the influence of the EMT or MET, as

$$\left(\mathbf{W}^n, \mathcal{P}^{\beta,n}\right) \longrightarrow \left(\mathbf{W}^{n+1/2}, \mathcal{P}^{\beta,n+1/2}\right) \tag{31a}$$

with

$$\mathbf{W}^{n+1/2} = \mathcal{N}^{\left[t^n, t^n + \frac{1}{2}\tau^n\right]}\left(\mathbf{W}^n, \mathcal{P}^{\beta,n}\right), \tag{31b}$$

$$\mathcal{P}^{\beta,n+1/2} = \left\{ \left(\mathbf{x}_p^{\beta,n+1/2}, m_p^{\beta,n+1/2}\right),\ p \in P^{n+1/2} \right\}, \tag{31c}$$

where $\mathcal{N}^{[t,t+\tau]}$ is the numerical solution operator responsible for the spatiotemporal evolution of the system (1a)–(1c) —without EMT and MET. Here, $x_p^{\beta,n+1/2}$, $p \in P^n$, is given by the half-step Euler-Maruyama particle motion scheme (8), re-written here with respect to the local variables

$$\mathbf{X}_p^{\beta,n+1/2} = \mathbf{X}_p^{\beta,n} + \mathbf{A}\left(\mathbf{X}_p^{\beta,n}\right)\frac{\tau^n}{2} + \mathbf{B}\left(\mathbf{X}_p^{\beta,n}\right) \cdot \mathbf{Z}_p \sqrt{\frac{\tau^n}{2}}. \tag{32}$$

The number of cell-particles, their indices and masses remain unchanged during this step $[t^n, t^n + \frac{1}{2}\tau^n]$, i.e.

$$P^{n+1/2} = P^n \quad \text{and} \quad m_p^{\beta,n+1/2} = m_p^{\beta,n}, \quad \forall p \in P^n.$$

Altogether, the combined evolution operators of the densities and cell-particles read for this time period as:

$$\mathcal{M}_{\frac{1}{2}\tau^n}\left(\mathbf{W}^n,\, \mathcal{P}^{\beta,n}\right) = \left(\mathbf{W}^{n+1/2},\, \mathcal{P}^{\beta,n+1/2}\right). \tag{33}$$

— At $t = t^n + \frac{1}{2}\tau^n$, the EMT and MET processes take place; they are assumed to be *instantaneous* and *tautochrone*. They are represented by the $\mathcal{R}^{\mathrm{EMT}}$ and $\mathcal{R}^{\mathrm{MET}}$ operators introduced in (28) and (30) respectively. For consistency, we scale them by the time step τ^n and change their notation to $\mathcal{R}_{\tau^n}^{\mathrm{EMT}}$ and $\mathcal{R}_{\tau^n}^{\mathrm{MET}}$, respectively.

In effect, the tuple $\left(\mathbf{W}^{n+1/2},\, \mathcal{P}^{\beta,n+1/2}\right)$ develops as

$$\left(\tilde{\mathbf{W}}^{n+1/2},\, \tilde{\mathcal{P}}^{\beta,n+1/2}\right) = \mathcal{R}_{\tau^n}\left(\mathbf{W}^{n+1/2},\, \mathcal{P}^{\beta,n+1/2}\right), \tag{34}$$

where $\mathcal{R}_{\tau^n}$ denotes the parallel application of $\mathcal{R}_{\tau^n}^{\mathrm{EMT}}$ and $\mathcal{R}_{\tau^n}^{\mathrm{MET}}$[4].

[4]Note that $\mathcal{R}_{\tau^n}^{\mathrm{EMT}}$ acts on the EC density and $\mathcal{R}_{\tau^n}^{\mathrm{MET}}$ acts on the MC cell-particles.

— During $[t^n + \frac{1}{2}\tau^n, t^{n+1}]$, the densities and cell-particles evolve again without the influence of EMT and MET as

$$\left(\tilde{\mathbf{W}}^{n+1/2},\, \tilde{\mathcal{P}}^{\beta,n+1/2}\right) \longrightarrow \left(\mathbf{W}^{n+1},\, \mathcal{P}^{\beta,n+1}\right),$$

where, in a similar way as in $[t^n, t^n + \frac{1}{2}\tau^n]$,

$$\mathbf{W}^{n+1} = \mathcal{N}^{\left[t^n+\frac{1}{2}\tau^n, t^{n+1}\right]}\left(\mathbf{W}^{n+1/2},\, \tilde{\mathcal{P}}^{\beta,n+1/2}\right), \tag{35}$$

$$\mathcal{P}^{\beta,n+1} = \left\{\left(\mathbf{x}_p^{\beta,n+1}, m_p^{\beta,n+1}\right),\ p \in P^{n+1}\right\}. \tag{36}$$

Again, $\mathcal{N}^{\left[t^n+\frac{1}{2}\tau^n, t^{n+1}\right]}$ represents the numerical method for the solution of the system (1a)–(1c),

$$P^{n+1} = P^{n+1/2} \quad \text{and} \quad m_p^{\beta,n+1} = m_p^{\beta,n+1/2}, \quad \forall p \in P^{n+1}.$$

In the above, $\mathbf{x}_p^{\beta,n+1}$, $p \in P^{n+1/2}$, is given by the half-step Euler-Maruyama scheme (8)

$$\mathbf{X}_p^{\beta,n+1} = \mathbf{X}_p^{\beta,n+1/2} + \mathbf{A}\left(\mathbf{X}_p^{\beta,n+1/2}\right)\frac{\tau^n}{2} + \mathbf{B}\left(\mathbf{X}_p^{\beta,n+1/2}\right)\cdot \mathbf{Z}_p\sqrt{\frac{\tau^n}{2}}. \tag{37}$$

We combine the two evolution operators as:

$$\mathcal{M}_{\frac{\tau}{2}}\left(\tilde{\mathbf{W}}^{n+1/2},\, \tilde{\mathcal{P}}^{\beta,n+1/2}\right) = \left(\mathbf{W}^{n+1},\, \mathcal{P}^{\beta,n+1}\right). \tag{38}$$

Overall, using (33), (34), and (38), we can write the combined evolution operator for the time period $[t^n, t^{n+1}]$ as a splitting method of the form

$$\left(\mathbf{W}^{n+1},\, \mathcal{P}^{\beta,n+1}\right) = \mathcal{M}_{\frac{\tau^n}{2}}\ \mathcal{R}_{\tau^n}\ \mathcal{M}_{\frac{\tau^n}{2}}\left(\mathbf{W}^{n},\, \mathcal{P}^{\beta,n}\right). \tag{39}$$

We close the system (39) with *no-flux boundary conditions* for the EC and MMP densities, and *reflective boundary conditions* for the MCs cell-particles. The latter should be understood as follows: each particle that escapes the domain Ω is returned to its last position within the domain, and its new direction is chosen randomly. As the ECM is modelled as an immovable part of the system, it does not translocate, hence no boundary conditions are employed.

3. Experiments and simulations. We perform three numerical experiments that exhibit the dynamics and the combination of the two cancer cell phenotypes and the transitions between the continuum and particle phases. For simplicity, we consider a constant diffusion coefficient σ in (7a) for the random part of the cell motion, and a drift coefficient μ depending on the gradient of the ECM, i.e. $\mu = \alpha\nabla v$, to address the directed part of their motion.

The discretization grids used for the numerical solution and simulations of (39) should not be confused with the partitioning of Ω in $\{M_i,\ i \in I\}$ as in (11). The former are used to solve the system (1a)-(1c) and are subject to mesh refinements. The latter are used for the back-and-forth transitions between the density and particle phases of the biological cells and are fixed, with sizes given equivalent to the reference cell K_0.

The implementations of numerical schemes and algorithms, and the simulations of the experiments included in this paper have been conducted in MATLAB [2015].

TABLE 1
Parameters and units corresponding to Experiment 3.1 and Fig. 5.

description	symbol	values and units
EC dens. diff. coef.	D_α	0 $\mathrm{cm}^2\mathrm{d}^{-1}$
EC dens. prol. coef.	ρ^α	0 d^{-1}
MC part. diff. coef.	$\lvert\mathbf{B}\rvert$	1.6 $\mathrm{cm}^2\mathrm{d}^{-1}$
MC part. hapt. coef.		30 $\mathrm{cm}^3\mathrm{mol}^{-1}\mathrm{d}^{-1}$
MC part. ref. mass	m_{ref}	1×10^{-5} gr
MC part. ref. diam.		1×10^{-2} cm
EMT prob.		5×10^{-4}
EMT rate	μ_a	1×10^{3}
MET prob.		0
MMP diff. coef.	D_m	0
ECM EC dens. degr.	λ_v^α	0 $\mathrm{cm}^2\mathrm{mol}^{-1}\mathrm{d}^{-1}$
ECM MC dens. degr.	λ_v^β	0 $\mathrm{cm}^2\mathrm{mol}^{-1}\mathrm{d}^{-1}$

Experiment 3.1 (EMT and particle flow). We set $\Omega = [-1,1]^2$ and consider the initial EC density

$$c^\alpha(\mathbf{x},0) = \left(e^{-5(x_1^2+x_2^2)} - 0.7\right)^+, \tag{40a}$$

with $\mathbf{x} = (x_1, x_2) \in \Omega$, where $(\cdot)^+$ denotes the positive part function. The ECM is non-uniform and exhibits a gradient towards the upper-right part of the domain

$$v(\mathbf{x},0) = 0.045\,(2x_1 + 3x_2) + 0.45. \tag{40b}$$

Initially, no MC cell-particles nor MMPs are present.

The parameters for this experiment are given in Table 1 and the results of the simulation are shown in Fig. 5. There is no particular biological justification for the parameter values and initial conditions in this experiment.

The phenomena observed in this experiment are the following: the ECs undergo EMT to MCs and new cell-particles appear in the system. The cell-particles "sense" the gradient of the ECM and respond haptotactically to it. This is included in the model and simulations via the advection velocities $\mathbf{v}$ of the cell-particles, see e.g. (9). Their motion incorporates also a random component; the resulting migration is a biased-random motion. The simplified EMT that we assume in this experiment takes place in every partition cell K_i, $i \in I$ with a probability that is denoted as "EMT prob." in Table 1. The set union of all partition cells where EMT takes place defines the set $\mathcal{E}$ that appears in (1a). The rate μ_a at which the EMT occurs in $\mathcal{E}$ is a given constant. In this experiment, we do not assume proliferation of the ECs, nor MET. Hence, the losses of the EC density, due to the EMT, appear as "holes" in their density profile and are not replenished with time. Moreover, the ECs do not actively migrate or otherwise translocate as (1a) includes neither haptotaxis nor diffusion (have set $D_\alpha = 0$ in this experiment), see Table 1.

Experiment 3.2 (Self-generated gradient). A typical phenomenon that macroscopic cancer invasion models exhibit, is the appearance of a propagating front that invades the ECM faster than the rest of the tumour, see e.g Byrne et al. [1999], Chaplain and Lolas [2005], Sfakianakis et al. [2017]. This front is followed by an intermediate distribution of the density, whereas the bulk of the tumour lags further behind. This phenomenon is due primarily to the degradation of either an extracellular chemical (in the case of a self-generated chemical gradient), or of the ECM (in the case of a

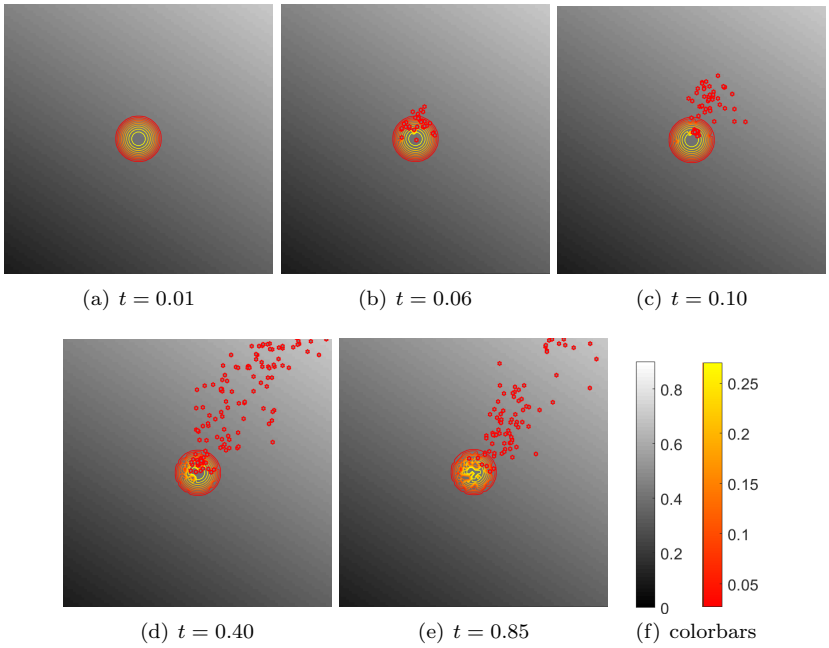

(a) $t = 0.01$ (b) $t = 0.06$ (c) $t = 0.10$

(d) $t = 0.40$ (e) $t = 0.85$ (f) colorbars

FIG. 5. *Experiment 3.1 (EMT and flow). Shown here is the time evolution of an initial EC density (isolines) and the resulting (after EMT) MC cell-particles (stars) over an ECM (background) that exhibits a directed gradient. The domain is* $\Omega = [-1, 1]^2$. *(a): An initial circular EC tumour resides over an ECM that exhibits a gradient towards the north-east direction. (b): The EC density undergoes EMT and gives rise to MC cell-particles. (c): Due to the diffusion and the haptotaxis, the cell-particles escape the initial tumour and migrate along the gradient of the ECM. (d): No proliferation is assumed for the ECs, hence the losses of their densities, due to the EMT towards MCs, are not replenished. This gives rise to "holes" in the initial tumour. (e): The phenomenon continues as long as parts of the EC density transform to MC cell-particles. (f): Common colorbars for the ECM (left) and the EC densities (right) in all sub-figures. See Table 1 for the parameters for this experiment.*

self-generated haptotaxis gradient) by the cancer cells. Such phenomena have been observed previously both in mathematical models and biological experiments, see e.g. Tweedy et al. [2016], Anderson et al. [2000].

In this experiment we exhibit the ability of our cell-particle submodel to reproduce such phenomena. In particular, we show that as the cancer cells (considered here as cell-particles) degrade the ECM, they induce a gradient on it and subsequently respond to this gradient by performing a directed and sustainable invasion. Most notably they form an isolated propagating front that invades the ECM.

For this experiment we consider the domain $\Omega = [-0.5, 0.5] \times [0, 2]$, over which lies a uniform ECM

$$v(\mathbf{x}, 0) = 0.1, \quad \mathbf{x} \in \Omega. \tag{41}$$

On the upper part of the domain, an initial EC density is assumed to be given by

$$c^{\alpha}(\mathbf{x}, 0) = 10^{-4} \mathcal{X}_{S_1}(\mathbf{x}), \quad \mathbf{x} \in \Omega, \tag{42}$$

TABLE 2
Parameters and units corresponding to Experiment 3.2 and Fig. 6.

description	symbol	values and units
EC dens. diff. coef.	D_α	0 $\mathrm{cm}^2\mathrm{d}^{-1}$
EC dens. prol. coef.	ρ^α	0 d^{-1}
MC part. diff. coef.	$\lvert\mathbf{B}\rvert$	2×10^{-2} $\mathrm{cm}^2\mathrm{d}^{-1}$
MC part. hapt. coef.		1×10^{-3} $\mathrm{cm}^3\mathrm{mol}^{-1}\mathrm{d}^{-1}$
MC part. ref. mass	m_{ref}	3×10^{-9} gr
MC part. ref. diam.		1×10^{-3} cm
EMT prob.		1
EMT rate	μ_a	10
MET prob.		0
MMP diff. coef.	D_m	0
ECM EC dens. degr.	λ_v^α	20 $\mathrm{cm}^2\mathrm{mol}^{-1}\mathrm{d}^{-1}$
ECM MC dens. degr.	λ_v^β	200 $\mathrm{cm}^2\mathrm{mol}^{-1}\mathrm{d}^{-1}$

with $S_1 = \left\{\mathbf{x} = (x_1, x_2) \in \Omega \,\middle|\, x_2 > 0.01\sin(5\pi x_1) + 1.97\right\}$. Before the beginning of the simulation, the EC density $c^\alpha(\mathbf{x}, 0)$ is completely transformed into MC cell-particles. As no MET takes place in this experiment, the MC cell-particles do not transition back to ECs. The MCs secrete MMPs that participate in the degradation of the ECM. The corresponding modelling parameters are given in Table 2 and the simulation results in Fig. 6.

In view of (8), all cell-particles perform a biased random motion; since the ECM is initially uniform, this motion is purely Brownian. As the cell-particles degrade the ECM, a gradient is formed in the matrix. The cell-particles found closer to this "interface" sense the gradient and respond haptotactically to it. This is encoded in the model through the dependence of the advection operator $\mathbf{A}$ on the particle velocity v, e.g. (9), which in turn depends on the gradient of the ECM at the current position of the particle. The directed part of their motion dominates and drives the cell-particles to higher matrix densities. As the cell-particles continue their invasion of the ECM they keep producing MMPs, degrading the ECM, and following the newly created gradient. Their motion is persistent in direction and speed.

With our model, we can now address particular questions of experimental interest: What is the minimum number of cancer cells needed to induce and sustain an invasion of the ECM persistent in direction and speed? How does the remodelling of the matrix affect the self-generated gradient motion? Such questions would among others serve as a bridge between experimental observations and mathematical models. Their study has to be the topic of a follow-up work, where the relevant experimental data should be analysed, as was done, for example, in Yang et al. [2016].

Experiment 3.3 (ECM invasion). This experiment is motivated by the *organotypic invasion assays* where cancer cells are plated over a collagen gel that contains healthy tissue, and where their invasion is studied over time, see for example Nyström et al. [2005], Valster et al. [2005] and Fig. 7.

We employ the complete set of dynamics of the system and consider the domain $\Omega = [-2, 2]^2$ occupied by an ECM of initial density $v(\mathbf{x}, 0)$ constructed by 64 randomly chosen extremal values per direction that are interpolated in a piecewise linear way. Small perturbations of the form of additive Gaussian noise are also included.

An initial density of ECs is given in the upper part of the domain as

$$c^\alpha(\mathbf{x}, 0) = 0.05\,\mathcal{X}_{S_2}(\mathbf{x})\,, \quad \mathbf{x} \in \Omega, \tag{43}$$

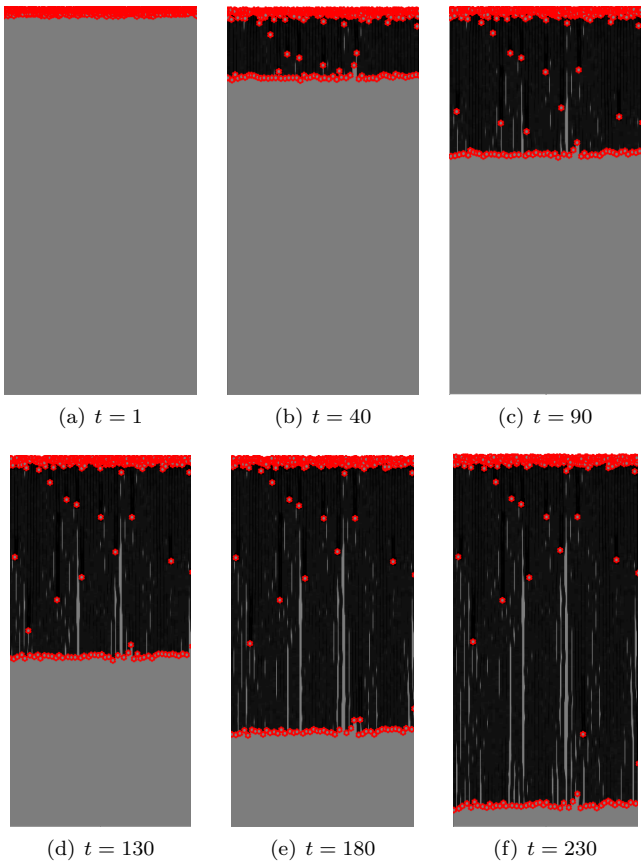

(a) $t = 1$ (b) $t = 40$ (c) $t = 90$

(d) $t = 130$ (e) $t = 180$ (f) $t = 230$

FIG. 6. *Experiment 3.2 (Self-generated gradient). Shown here is the migration of a number of MC cell-particles (stars) over an ECM (background landscape) in the absence of MET and EMT. The directed migration of the MC cell-particles is due to their haptotactic response to the gradients of the ECM that the MC cell-particles have induced. The domain is* $\Omega = [-0.5, 0.5] \times [0, 2]$. *(a): The MC cell-particles reside over an initially uniform ECM. Their migration is mostly Brownian. (b)-(c): The cell-particles degrade the matrix and introduce a gradient which is sensed by the cell-particles that are closer to the "interface". In effect, their motion is driven mostly by haptotaxis. As the cells invade the ECM, they continue to degrade the matrix and follow the new gradient that they have induced. (d)-(f): The migration of the cell-particles in the front is persistent in direction and speed, while the cell-particles in the rear (where the ECM is depleted) perform mostly a Brownian motion.*

with $S_2(\mathbf{x}) = \left\{\mathbf{x} = (x_1, x_2) \in \Omega \,\middle|\, x_2 > 0.05\sin(5\pi x_1) + 0.05\, x_1 + 1.1\right\}$. Initially, neither MC cell-particles nor MMPs exist in the system. The parameters for this experiment can be found in Table 3 and the simulation results are presented in Fig. 8.

The ECs proliferate and diffuse, but most notably transform via EMT to MC cell-particles. These MC cell-particles do not proliferate but they are very aggressive in their motility. As they escape the main body of the tumour, they undergo MET back to ECs. As a result, new EC concentrations appear, they grow due to proliferation, and give rise to tumour "islands". These "islands" merge with each other as well as with the main body of the tumour. The main characteristic and novelty of our hybrid

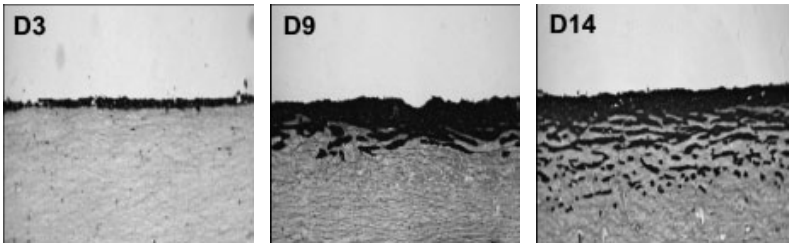

FIG. 7. *Timecourse (days 3, 9, and 14) study of the invasion of squamus carcinoma cells (black matter) on an organotypic assay with human fibroblast cells (gray matter). The invasion occurs in the form of cancer cell "islands" formed in front of the main body of the tumour. We reproduce the same phenomenon in the invasion Experiment 3.3 and in Fig. 8. These images are taken from Nyström et al. [2005] (PERMISSION REQUESTED).*

TABLE 3
Parameters, units, and sourses corresponding to Experiment 3.3 and Fig. 8.

description	symbol	values and units	sources
EC dens. diff. coef.	D_α	3.456×10^{-6} cm^{2}d^{-1}	Chaplain and Lolas [2005]
EC dens. prol. coef.	ρ^α	1.2 d^{-1}	Orme and Chaplain [1997]
MC part. diff. coef.	$\|\mathbf{B}\|$	3×10^{-1} cm^{2}d^{-1}	Stokes and Lauffenburger [1998]
MC part. hapt. coef.		3 cm^{3}mol^{-1}d^{-1}	(estimate)
MC part. ref. mass	m_{ref}	3×10^{-9} gr	B10NUMB3R5 (HeLa cell)
MC part. ref. diam.		1×10^{-3} cm	B10NUMB3R5 (HeLa cell) & Zhao et al. [2008]
EMT prob.		1×10^{-5}	(estimate)
EMT rate	μ_a	4×10^{-3}	(estimate)
MET prob.		2×10^-2	(estimate)
MMP diff. coef.	D_m	0	
ECM EC dens. degr.	λ_v^α	1×10^{-5} cm^{2}mol^{-1}d^{-1}	Anderson and Chaplain [1998]
ECM MC dens. degr.	λ_v^β	1×10^{-4} cm^{2}mol^{-1}d^{-1}	Anderson and Chaplain [1998]

model, is that it predicts the emergence of these tumour "islands" outside of the main body of the tumour.

The growth of the tumour with the combined dynamics of the ECs and MCs possesses several interesting properties. The tumour grows much faster than it would, if it was comprised only of the ECs. This is so, since the new EC "islands" that arise after the MCs have escaped the main body of the tumour undergo MET, exploit uninhabited locations, and grow "to all directions". On the contrary, in the main body of the tumour, only the ECs found in the periphery contribute to the growth of its support.

Moreover, the independent and aggressive migration of MCs provides them with faster access to the circulatory network and the possibility to translocate to secondary places within the organism. As the MCs possess the ability to give rise to EC "islands" at the new locations, new tumours might appear, and *metastasis* will have occurred. Although it is not our aim in the current paper to reproduce particular experimental scenarios, a direct comparison of the simulation results in Fig. 8 with the organotypic assay images in Fig. 7 exhibits clearly that this phenomenon is reproduced by our model.

Another sought-after property in cancer invasion modelling is that the MCs remain undetected while they invade the ECM. It is not until a new ECs tumour has been established that it can grow to be of any detectable size. Again, this property is inherently built in our modelling approach.

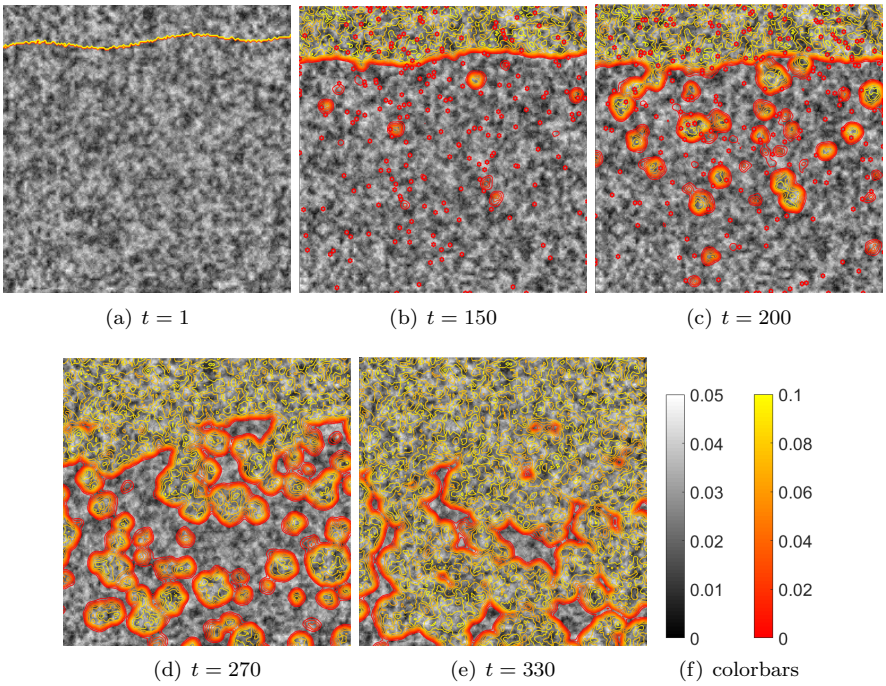

(a) $t = 1$ (b) $t = 150$ (c) $t = 200$

(d) $t = 270$ (e) $t = 330$ (f) colorbars

FIG. 8. *Experiment 3.3 (ECM invasion). Shown here is the time evolution of the ECM (background landscape), the EC (isolines), and the MC cell-particles (stars) over the domain* $\Omega = [-2, 2]^2$. *(a): According to their modelling dynamics, an initial uniform density of ECs evolves according to system (1a)–(1c), and mostly proliferates rather than diffuses. (b)-(c): The MC cell-particles that are produced through the EMT escape the main body of the tumour, invade the ECM, undergo MET and eventually give rise to new EC "islands". (d)-(e): These "islands" grow mostly due to proliferation and eventually merge with the main body of the tumor. (f): The colorbars for the ECM (left) and the EC density (right) are common to all figures.*

4. Discussion. We present in this work a modelling framework to study the combined invasion of the ECM by two types of cancer cells, the ECs and MCs. The proposed framework is a *genuinely multiscale hybrid model* that treats the ECs in a macroscopic and deterministic manner and the MCs in an atomistic and stochastic way. It has similarities with, and develops further along the lines laid, e.g., in Anderson et al. [2000], Anderson [2005], Colombi et al. [2017].

Cornerstone to our modelling approach is the remark that the MCs are much fewer than the ECs and that they emanate from the ECs via a dynamic EMT cellular differentiation program. We also assume that the MCs give rise, via the opposite MET-like cellular program, to ECs; a key property in the metastasis of the tumour. For the sake of simplicity, we assume that both types of cancer cells perform a random motion, and that the MCs are much more aggressive in their migration than the ECs. Clearly, more complex and biologically relevant assumptions can be placed on the cancer cells.

We encode this information through a hybrid approach: The spatiotemporal evolution of the ECs, the ECM, the MMPs, and the rest of the environmental components are dictated by the macroscopic deterministic model (1a)–(1c). Namely, the ECs are

assumed to diffuse and proliferate. The MMPs are assumed to be produced by the cancer cells and degrade the ECM, and the ECM in turn, is assumed to be non-uniform and is not remodelled. The MCs on the other hand are considered as separate cell-particles that obey a system of SDEs, (7a), that accounts for *haptotaxis* and *random motion* for each MC.

The (combined) evolution of the two types of cancer cells is coupled through transitions between the EMT and MET. The triggering mechanisms of EMT and MET are quite complex and involve the action of several biochemical components such as TGF-β, EGF, and more. For the purpose of clarity of the presentation, we follow in this work a simplified approach and assume that the EMT and MET occur randomly over the ECs and MCs respectively, cf. Section 2.4. The EMT and MET programmes are realised through the *density-to-particle* and *particle-to-density* operators given in (17) and (21).

Our modelling approach allows to reproduce several biologically relevant phenomena encountered in the invasion of cancer that are not easily addressed with the usual modelling approaches. Our focus though in this work lies with the description and the handling of the mathematical model and the numerical method; we only present here basic biological situations and postpone the more elaborate investigations for a follow-up work.

With the atomistic component of our model, we are able to reproduce a sustainable invasion of the ECM by means of a *self-induced haptotaxis gradient* as shown in Experiment 3.2. Such behaviour is observed in biological situations, e.g. Tweedy et al. [2016], and becomes crucial to several biological processes like *wound healing*. The detailed study of such cases falls beyond the scope of the current paper; here we use this experiment as an indication that our model can reproduce biologically relevant situations. At the same time it serves as verification of the propagating invasion front seen in simulations of macroscopic deterministic cancer invasion models, e.g., Anderson and Chaplain [1998], Chaplain and Lolas [2005], Sfakianakis et al. [2017].

With the full model, we are able to reproduce the spread of the tumour and the invasion of the ECM in the form of invasion "islands", Japanese Gastric Cancer Association [2011], Ito et al. [2012], Masuda et al. [2017] and Experiment 3.3. These are well known to appear in many cases of cancer and are quite challenging to reproduce by either macroscopic or atomistic cancer invasion models, e.g., Domschke et al. [2014b], Hiremath and Surulescu [2016b]. With our approach these invasion "islands" are an emergent process of our modelling framework and—most notably—they appear outside the main body of the tumour.

What is also natural in our approach, is that the MC cell-particles escape the main body of the tumour and *remain undetected* while they invade the ECM. It is only after they have established new "islands" in the vicinity of the original tumour or in another location within the organism that they can be detected. This is another sought-after property in the field of cancer invasion modelling.

For the sake of presentation, we have only considered here some of the fundamental properties of cancer growth that our model can reproduce, see (1a)–(1c). Still they suffice to warrant extensions and investigations of more realistic biological situations and experimental settings. To mention but a few: extension to the more realistic three-dimensional space, more realistic EMT and MET transitions, interactions between

cancer cells of the same and different types including collisions, adhesions, short or long range interactions, and the *collective behaviour* of cancer cells.

Data Management. All the computational data output is included in the present manuscript.

Acknowledgements. NS was partly funded from the German Science Foundation (DFG) under the grant SFB 873: "Maintenance and Differentiation of Stem Cells in Development and Disease". For the work AM is partly supported by funding from the European Union Horizon 2020 research and innovation programme under the Marie Skłodowska-Curie grant agreement No 642866, the Commission for Developing Countries, and was partially supported by a grant from the Simons Foundation. AM is a Royal Society Wolfson Research Merit Award Holder funded generously by the Wolfson Foundation. The authors (NS, AM, MC) would also like to thank the Isaac Newton Institute for Mathematical Sciences for its hospitality during the programme [Coupling Geometric PDEs with Physics for Cell Morphology, Motility and Pattern Formation] supported by EPSRC Grant Number EP/K032208/1.

Supplementary Material. Two simulations that correspond to Experiments 3.2 and 3.3, i.e. `Self_generated_gradient` and `ECM_invasion` respectively.

References.

D. Hanahan and R.A. Weinberg. The Hallmarks of Cancer. *Cell*, 100:57–70, 2000.

D. Hanahan and R.A. Weinberg. The Hallmarks of Cancer: The next generation. *Cell*, 144: 646–671, 2011.

P. Mehlen and A. Puisieux. Metastasis: a question of life or death. *Nat. Rev. Cancer*, 6: 449–58, 2006.

B. Weigelt, J.L. Peterse, and L.J. van't Veer. Breast cancer metastasis: markers and models. *Nat. Rev. Cancer*, 8:591–602, 2005.

P. Friedl and K. Wolf. Tumour-cell invasion and migration: diversity and escape mechanisms. *Nat. Rev. Cancer*, 5:362–74, 2003.

J.P. Thiery. Epithelial–mesenchymal transitions in tumour progression. *Nat. Rev. Cancer*, 2(6):442–454, 2002.

J. Roche. The epithelial-to-mesenchymal transition in cancer. *Cancers*, 10:1420–1428, 2018.

R. Kalluri and R. A. Weinberg. The basics of epithelial-mesenchymal transition. *J. Clin. Invest.*, 6:1420–1428, 2009.

V. Te Boekhorst, L. Preziosi, and P. Friedl. Plasticity of cell migration in vivo and in silico. *Ann. Rev. Cell Dev. Biol.*, 32:, 491–526, 2016.

C.D. Madsen and E. Sahai. Cancer dissemination–lessons from leukocytes. *Dev. Cell*, 19: 13–26, 2010.

F. Sabeh, R. Shimizu-Hirota, and S.J. Weiss. Protease-dependent versus -independent cancer cell invasion programs: three-dimensional amoeboid movement revisited. *J. Cell Biol.*, 185: 11–9, 2009.

R.A. Gatenby and E.T. Gawlinski. A reaction-diffusion model of cancer invasion. *Cancer Res.*, 56:5745–53, 1996.

I. Ramis-Conde, M.A.J. Chaplain, and A.R.A. Anderson. Mathematical modelling of cancer cell invasion of tissue. *Math. Comput. Modell.*, 47:533–545, 2008a.

I. Ramis-Conde, D. Drasdo, M.A.J. Chaplain, and A.R.A. Anderson. Modelling the influence of the e-cadherin - β-catenin pathway in cancer cell invasion and tissue architecture: A multi-scale approach. *Biophys. J.*, 95:155–165, 2008b.

H. Hatzikirou, L. Bruscha, C. Schaller, M. Simon, and A. Deutsch. Prediction of traveling front behavior in a lattice-gas cellular automaton model for tumor invasion. *Comput. Math. Appl.*, 59:2326–2339, 2010.

J. Wang, L. Zhang, C. Jing, G. Ye, H. Wu, H. Miao, Y. Wu, and X. Zhou. Multi-scale

agent-based modeling on melanoma and its related angiogenesis analysis. *Theor. Biol. Med. Model.*, 10:41, 2013.

D.K. Schlüter, I. Ramis-Conde, and M.A.J. Chaplain. Multi-scale modelling of the dynamics of cell colonies: insights into cell adhesion forces and cancer invasion from in silico simulations. *J. R. Soc. Interface*, 12, 2015. doi: 10.1098/rsif.2014.1080.

M.A.J. Chaplain and M.E. Orme. Travelling waves arising in mathematical models of tumour angiogenesis and tumour invasion. *FORMA*, 10:147–170, 1996.

L. Preziosi. *Cancer Modelling and Simulation*. Chapman and Hall/CRC, 2003.

M.A.J. Chaplain and G. Lolas. Mathematical modelling of cancer cell invasion of tissue: the role of the urokinase plasminogen activation system. *Math. Modell. Methods. Appl. Sci.*, 15:1685–1734, 2005.

M.A.J. Chaplain and G. Lolas. Mathematical modelling of cancer invasion of tissue: Dynamic heterogeneity. *Net. Hetero. Med.*, 1:399–439, 2006.

V. Andasari, A. Gerisch, G. Lolas, A.P. South, and M.A.J. Chaplain. Mathematical modelling of cancer cell invasion of tissue: biological insight from mathematical analysis and computational simulation. *J. Math. Biol.*, 63(1):141–71, 2011.

P. Domschke, D. Trucu, A. Gerisch, and M.A.J. Chaplain. Mathematical modelling of cancer invasion: Implications of cell adhesion variability for tumour infiltrative growth patterns. *J. Theor. Biol.*, 361:41–60, 2014a.

N.E. Deakin and M.A.J. Chaplain. Mathematical modeling of cancer invasion: the role of membrane- bound matrix metalloproteinases. *Front. Oncol.*, 3:70, 2013.

K.J. Painter and T. Hillen. Mathematical modelling of glioma growth: the use of Diffusion Tensor Imaging (DTI) data to predict the anisotropic pathways of cancer invasion. *J. Theor. Biol.*, 323:25–39, 2013.

N. Kolbe, J. Katuchova, N. Sfakianakis, N. Hellmann, and M. Lukacova-Medvidova. A study on time discretization and adaptive mesh refinement methods for the simulation of cancer invasion: The urokinase model. *Appl. Math. Comput.*, 273:353–376, 2016.

N. Sfakianakis, N. Kolbe, N. Hellmann, and M. Lukacova-Medvidova. A multiscale approach to the migration of cancer stem cells: Mathematical modelling and simulations. *Bull. Math. Biol.*, 79:209–235, 2017.

C. Engwer, C. Stinner, and C. Surulescu. On a structured multiscale model for acid-mediated tumor invasion: The effects of adhesion and proliferation. *Math. Models Methods Appl. Sci.*, 27:1355, 2017.

L. Peng, D. Trucu, P. Lin, A. Thompson, and M.A.J. Chaplain. A multiscale mathematical model of tumour invasive growth. *Bull. Math. Biol.*, 79:389–429, 2017.

A.R.A. Anderson, M.A.J. Chaplain, E.L. Newman, R.J. C. Steele, and A.M. Thompson. Mathematical modelling of tumour invasion and metastasis. *J. Theor. Medicine*, 2:129–154, 2000.

A.R.A Anderson. A hybrid mathematical model of solid tumour invasion: the importance of cell adhesion. *Math. Med. Biol.*, 22:163–186, 2005.

A. Colombi, M. Scianna, and L. Preziosi. Coherent modelling switch between pointwise and distributed representations of cell aggregates. *J. Math. Biol.*, 74(4):783–808, 2017.

A. Colombi, M. Scianna, and A. Tosin. Differentiated cell behavior: a multiscale approach using measure theory. *J. Math. Biol.*, 71(5):1049–1079, 2015a.

A. Colombi, M. Scianna, and L. Preziosi. A measure-theoretic model for collective cell migration and aggregation. *Math. Model. Nat. Phenom.*, 10(1):4–35, 2015b.

V. Capasso and D. Morale. On the stochastic modelling of interacting populations. a multiscale approach leading to hybrid models. In W. Fitzgibbon, Y.A. Kuznetsov, P. Neittaanmäki, J. Périaux, and O. Pironneau, editors, *Applied and Numerical Partial Differential Equations: Scientific Computing in Simulation, Optimization and Control in a Multidisciplinary Context*, pages 59–80. Springer Netherlands, Dordrecht, 2010.

S.A. Hiremath and C. Surulescu. A stochastic model featuring acid-induced gaps during tumor progression. *Nonlinearity*, 29(3):851, 2016a.

S.A. Hiremath, C. Surulescu, A. Zhigun, and S. Sonner. On a coupled sde-pde system

modeling acid-mediated tumor invasion. *Discrete Cont. Dyn.-B*, 23:3685, 2018.
A. Colombi and M. Scianna. Modelling human perception processes in pedestrian dynamics: a hybrid approach. *R. Soc. Open Sci.*, 4:1049–1079, 2017.
J.-A. Cañizo, J.-A. Carrillo, and F.S. Patacchini. Existence of compactly supported global minimisers for the interaction energy. *Arch. Ration. Mech. An.*, 217(3):1197–1217, 2015.
J.-A. Carrillo, A. Colombi, and M. Scianna. Adhesion and volume constraints via nonlocal interactions determine cell organisation and migration profiles. *J. Theor. Biol.*, 445:75 – 91, 2018.
L.A Liotta, M.G. Saidel, and J. Kleinerman. Diffusion model of tumor vascularization and growth. *Bull. Math. Biol.*, 39:117–128, 1977.
M.H. Byrne, M.A.J. Chaplain, G.J. Pettet, and D.L.S. McElwain. A mathematical model of trophoblast invasion. *J. Theor. Medicine*, 1:275–286, 1999.
T. Hillen, K.J. Painter, and M. Winkler. Global solvability and explicit bounds for non-local adhesion models. *Eur. J. Appl. Math.*, 29:645–684, 2017.
A. Marciniak-Czochra and M. Ptashnyk. Boundedness of solutions of a haptotaxis model. *Math. Mod. Meth. Appl. S.*, 20:449–476, 2010.
J. Giesselmann, N. Kolbe, M. Lukacova-Medvidova, and N. Sfakianakis. Existence and uniqueness of global classical solutions to a two species cancer invasion haptotaxis model. *Discrete Cont. Dyn.-B*, 22:1, 2018.
Chr. Stinner, Chr. Surulescu, and A. Uatay. Global existence for a go-or-grow multiscale model for tumor invasion with therapy. *Mathematical Models and Methods in Applied Sciences*, 26:2163–2201, 08 2016.
A. Marciniak-Czochra, G. Karch, and K. Suzuki. Unstable patterns in reaction-diffusion model of early carcinogenesis. *J. Math. Pures Appl.*, 99:509–543, 2013.
M. Winkler and Y. Tao. Energy-type estimates and global solvability in a two-dimensional chemotaxis–haptotaxis model with remodeling of non-diffusible attractant. *J. Diff. Eq.*, 257:784–815, 2014.
F.H. Harlow. A machine calculation method for hydrodynamic problems. *LAMS*, 1965.
R.A. Gingold and J.J. Monaghan. Smoothed particle hydrodynamics: theory and application to non-spherical stars. *Mon. Not. R. Astron. Soc.*, 181:375–389, 1977.
R.I. Stratonovich. A new representation for stochastic integrals and equations. *SIAM J. Control*, 4(2):362–371, 1966.
X. Blanc, C. Le Bris, and P.-L. Lions. Atomistic to continuum limits for computational materials science. *Math. Mod. Num. Anal.*, 41:391–426, 2007.
P.K. Kitanidis. Particle-tracking equations for the solution of the advection-dispersion equation with variable coefficients. *Water Resour. Res.*, 30:3225–3227, 1994.
Ch. Makridakis, D. Mitsoudis, and Ph. Rosakis. On atomistic-to-continuum couplings without ghost forces in three dimensions. *Appl. Math. Res. Express*, 1:87–113, 2014.
A.F.B. Tompson and D.E. Dougherty. Patricle-grid methods for reacting flows in porous media with application to Fisher's equation. *Appl. Math. Modeling*, 16(7):374–383, 1992.
B. Oksendal. *Stochastic Differential Equations*. Springer-Verlag Berlin Heidelberg, 2003.
P.E. Kloeden and E. Platen. *Numerical Solution of Stochastic Differential Equations*. Springer Berlin Heidelberg, Berlin, 1992.
L. Arnold. *Stochastic Differential Equations: Theory and applications*. John Wiley, New York, 1974.
P.A. Raviart. Particle numerical models in fluid dynamics. In K.W. Morton and M.J. Baines, editors, *Numerical Methods for Fluid Dynamics*, pages 231–253. Clarendon Press, Oxford, 1986.
MATLAB. *MATLAB version 8.6.0 (R2015b)*. The MathWorks Inc., Natick, Massachusetts, 2015.
L. Tweedy, D.A. Knecht, G.M. Mackay, and R.H. Insall. Self-generated chemoattractant gradients: Attractant depletion extends the range and robustness of chemotaxis. *PLOS Biology*, 14(3):1–22, 2016.
F.W. Yang, Ch. Venkataraman, V. Styles, V. Kuttenberger, E. Horn, Z. von Guttenberg,

and A. Madzvamuse. A computational framework for particle and whole cell tracking applied to a real biological dataset. *J. Biomech.*, 49(8):1290–1304, 2016.
M. Nyström, G.J. Thomas, I.C. Stone, M. Mackenzie, I.R. Hart, and J.F. Marshall. Development of a quantitative method to analyse tumour cell invasion in organotypic culture. *J. Pathol.*, 205:468–475, 2005.
M.E. Orme and M.A.J. Chaplain. Two-dimensional models of tumour angiogenesis and anti-angiogenesis strategies. *IMA J. Math. Appl. Med. Biol.*, 14:189–205, 1997.
C.L. Stokes and D.A. Lauffenburger. Analysis of the roles of microvessel endothelial cell random motility and chemotaxis in angiogenesis. *J. Theor. Biol.*, 152:377–403, 1998.
L. Zhao, C.D. Kroenke, J. Song, D. Piwnica-Worms, J.J. Ackerman, and J.J. Neil. Intracellular water-specific mr of microbead-adherent cells: the hela cell intracellular water exchange lifetime. *NMR Biomed.*, 21(2):159–164, 2008.
A.R.A. Anderson and M.A.J. Chaplain. A mathematical model for capillary network formation in the absence of endothelial cell proliferation. *Appl. Math. Letters*, 11:109–114, 1998.
A. Valster, N.L. Tran, M. Nakada, M.E. Berens, A.Y. Chan, and M. Symons. Cell migration and invasion assays. *Methods*, 37:208–215, 2005.
Japanese Gastric Cancer Association. Japanese classification of gastric carcinoma: 3rd english edition. *Gastric Cancer*, 14(2):101–112, 2011.
Eisuke Ito, Soji Ozawa, Hiroshi Kijima, Akihito Kazuno, Takayuki Nishi, Osamu Chino, Hideo Shimada, Makiko Tanaka, Shigeaki Inoue, Sadaki Inokuchi, and Hiroyasu Makuuchi. New invasive patterns as a prognostic factor for superficial esophageal cancer. *J. Gastroenterol.*, 47(12):1279–1289, 2012.
R. Masuda, H Kijima, N. Imamura, and Y. Masuda D. Iwazaki M. Aruga, N. andakamura. Tumor budding is a significant indicator of a poor prognosis in lung squamous cell carcinoma patients. *Mol . Med. Rep.*, 6:937–943, 2017.
P. Domschke, D. Trucu, A. Gerisch, and M.A.J. Chaplain. Mathematical modelling of cancer invasion: Implications of celladhesion variability for tumour infiltrative growth patterns. *J. Theor. Biol.*, 361:41–60, 2014b.
S.A. Hiremath and C. Surulescu. A stochastic model featuring acid-induced gaps during tumor progression. *Nonlinearity*, 29:851, 2016b.
O. Lakkis, A. Madzvamuse, and Ch. Venkataraman. Implicit–explicit timestepping with finite element approximation of reaction–diffusion systems on evolving domains. *SIAM J. Numer. Anal.*, 51:2309–2330, 2012.
C.A. Kennedy and M.H. Carpenter. Additive Runge-Kutta schemes for convection-diffusion-reaction equations. *Appl. Numer. Math.*, 1(44):139–181, 2003.
A.N. Krylov. On the numerical solution of the equation by which in technical questions frequencies of small oscillations of material systems are determined. *Otdel. mat. i estest. nauk.*, VII(4):491–539, 1931.
H.A. van der Vorst. Bi-CGSTAB: A fast and smoothly converging variant of Bi-CG for the solution of nonsymmetric linear systems. *SIAM J. Sci. Comput.*, 13(2):631–644, 1992.
S.M. Iacus. *Simulation and Inference for Stochastic Differential Equations*. Springer, 2008.

Appendix A. (Numerical method for the ARD model (2)). We use a second order *Implicit-Explicit Runge-Kutta* (IMEX-RK) *Finite Volume* (FV) numerical method that was previously developed in Kolbe et al. [2016], Sfakianakis et al. [2017] where we refer for more details, see also Lakkis et al. [2012]. Here we provide some basic description of the method.

We consider a generic ARD system of the form

$$\mathbf{w}_t = A(\mathbf{w}) + R(\mathbf{w}) + D(\mathbf{w}), \tag{44}$$

where $\mathbf{w}$ represents the solution vector, and A, R, and D the *advection*, *reaction*, and *diffusion* operators respectively.

TABLE 4

Butcher tableaux for the explicit (upper) and the implicit (lower) parts of the third order IMEX scheme (47), see also Kennedy and Carpenter [2003].

0				
$\frac{1767732205903}{2027836641118}$	$\frac{1767732205903}{2027836641118}$			
$\frac{3}{5}$	$\frac{5535828885825}{10492691773637}$	$\frac{788022342437}{10882634858940}$		
1	$\frac{6485989280629}{16251701735622}$	$-\frac{4246266847089}{9704473918619}$	$\frac{10755448449292}{10357097424841}$	
	$\frac{1471266399579}{7840856788654}$	$-\frac{4482444167858}{7529755066697}$	$\frac{11266239266428}{11593286722821}$	$\frac{1767732205903}{4055673282236}$
0	0			
$\frac{1767732205903}{2027836641118}$	$\frac{1767732205903}{4055673282236}$	$\frac{1767732205903}{4055673282236}$		
$\frac{3}{5}$	$\frac{2746238789719}{10658868560708}$	$-\frac{640167445237}{6845629431997}$	$\frac{1767732205903}{4055673282236}$	
1	$\frac{1471266399579}{7840856788654}$	$-\frac{4482444167858}{7529755066697}$	$\frac{11266239266428}{11593286722821}$	$\frac{1767732205903}{4055673282236}$
	$\frac{1471266399579}{7840856788654}$	$-\frac{4482444167858}{7529755066697}$	$\frac{11266239266428}{11593286722821}$	$\frac{1767732205903}{4055673282236}$

We denote by $\mathbf{w}_h(t)$ the corresponding (semi-)discrete numerical approximation —indexed here by the maximal spatial grid diameter h— that satisfies the system of ODEs

$$\partial_t \mathbf{w}_h = \mathcal{A}(\mathbf{w}_h) + \mathcal{R}(\mathbf{w}_h) + \mathcal{D}(\mathbf{w}_h), \tag{45}$$

where the numerical operators $\mathcal{A}$, $\mathcal{R}$, and $\mathcal{D}$ are *discrete approximations* of the operators A, R, and D in (44) respectively.

Our method of choice for solving (45) is an *Implicit-Explicit Runge-Kutta* (IMEX-RK) method based on a *splitting* in explicit and implicit terms in the form

$$\partial_t \mathbf{w}_h = \mathcal{I}(\mathbf{w}_h) + \mathcal{E}(\mathbf{w}_h). \tag{46}$$

The actual splitting depends on the particular problem in hand but in a typical case, the advection terms $\mathcal{A}$ are treated explicitly in time, the diffusion terms $\mathcal{D}$ implicitly, and the reaction terms $\mathcal{R}$ partly explicit and partly implicit.

More precisely, we employ a diagonally implicit RK method for the implicit part, and an explicit RK for the explicit part

$$\begin{cases} \mathbf{W}_i^* = \mathbf{w}_h^n + \tau_n \sum_{j=1}^{i-2} \bar{a}_{i,j} \mathbf{E}_j + \tau_n \bar{a}_{i,i-1} \mathbf{E}_{i-1}, & i = 1 \dots s \\ \mathbf{W}_i = \mathbf{W}_i^* + \tau_n \sum_{j=1}^{i-1} a_{i,j} \mathbf{I}_j + \tau_n a_{i,i} \mathbf{I}_i, & i = 1 \dots s \\ \mathbf{w}_h^{n+1} = \mathbf{w}_h^n + \tau_n \sum_{i=1}^{s} \bar{b}_i \mathbf{E}_i + \tau_n \sum_{i=1}^{s} b_i \mathbf{I}_i \end{cases} \tag{47}$$

where $s = 4$ are the stages of the IMEX method, $\mathbf{E}_i = \mathcal{E}(\mathbf{W}_i)$, $I_i = \mathcal{I}(\mathbf{W}_i)$, $i = 1 \dots s$, $\{\bar{b}, \bar{A}\}$, $\{b, A\}$ are respectively the coefficients for the explicit and the implicit part of the scheme, given by the Butcher Tableau in Table 4, Kennedy and Carpenter [2003]. We solve the linear systems in (47) using the *iterative biconjugate gradient stabilised Krylov subspace* method Krylov [1931], van der Vorst [1992].

Appendix B. (An explicit numerical scheme for the SDE (7a)). We consider an Ito process $X = \{X_t, t_0 \le t \le T\}$ that satisfies the *Brownian motion* SDE

$$d\mathbf{X}_t = \alpha \mathbf{X}_t dt + \beta d\mathbf{W}_t, \tag{48}$$

where $\mathbf{X}_t$ denotes the position in space, and where $\alpha \in \mathbb{R}$ and $\beta > 0$ are constants.

We discretise (48) with the explicit Euler-Maruyama scheme as

$$\mathbf{X}_{n+1} = \mathbf{X}_n + \alpha \mathbf{X}_n \tau + \beta \Delta \mathbf{W}_t. \tag{49}$$

By setting $\Delta \mathbf{W}_t = \mathbf{Z}\sqrt{\tau}$ with $\mathbf{Z} \sim \mathbf{N}(0, 1)$, (49) reads

$$\mathbf{X}_{n+1} = \mathbf{X}_n + \alpha \mathbf{X}_n \tau + \beta \mathbf{Z}\sqrt{\tau} \tag{50}$$

which is a simpler version of the scheme that we employ in (8).

For further details on the numerical treatment of (48) and other SDEs we refer to Iacus [2008], Kloeden and Platen [1992].